Available online at www.sciencedirect.com
ScienceDirect
Nuclear Instruments and Methods in Physics Research B 260 (2007) 288–292
NIM B
Beam Interactions with Materials & Atoms
www.elsevier.com/locate/nimb

A review of transmission channelling using high-demagnification microprobes

M.B.H. Breese *, E.J. Teo, L. Huang

Physics Department, National University of Singapore, 10 Lower Kent Ridge Road, Singapore 119260, Singapore

Available online 3 April 2007

Abstract

Recent work on the implementation and applications of a transmission channelling facility on a high-demagnification microprobe is described. A new measurement geometry is used in which only the useful channelled protons are recorded and the large flux of nonchanneled protons, which convey little useful information, is not recorded. This results in transmission channelling images with greatly improved counting statistics with much lower statistical noise. The use of this new system to provide high-resolution, low-noise images of lattice defects such as stacking faults and misfit dislocations is demonstrated. A measurement system capable of providing transmission channelling imaging of lattice defects in real-time is described.

PACS: 61.85.+p; 61.72.−y; 41.85.−p; 07.78.+s

Keywords: Transmission ion channelling; Nuclear microprobe; Misfit dislocations; Stacking faults

1. Introduction

Focused MeV proton beams have been used for many years to produce spatially-resolved transmission channelling images of defects in thinned crystals [1–4]. In early measurements the energy spectrum of the transmitted protons was recorded with a semiconductor detector on the beam axis while the focused beam scans over the crystal surface, in a manner similar to scanning transmission ion microscopy images [5,6]. Channelled protons lose energy at typically half the rate of nonchanneled protons [7,8]. Any lattice disruption causes additional dechannelling [9,10] and transmission channelling images showing variations in transmitted energy reveal the distribution of defects such as misfit dislocations [3,4,11], stacking faults [12,13], copper oxide precipitates, exfoliated regions in smart-cut silicon wafers etc. Much of this work is described in [14].

A transmission channelling set-up was recently implemented on a high-demagnification triplet microprobe utilising quadrupole lenses in which parasitic fields [15] and many other aberrations which limit the beam spot size [14,16] have been eliminated. This gives a microprobe which is capable of focusing beams to about 30 nm [17,18], with demagnifications of about 60 and 220. Even in such a high-demagnification system the focused beam convergence angle used for transmission channelling measurements is only ~0.01°. This is still much less than the planar channelling critical angle of $\theta_c = 0.17°$ for 2 MeV protons in the silicon (1 1 0) planes owing to the very low beam currents of 1 fA to 1 pA used for analysis.

Many effects were not resolved though in this earlier transmission channelling analyses owing to insufficient spatial resolutions of 300 nm at best and small variations in transmitted energy, resulting in low-contrast, "noisy" images. Both these limitations have been overcome [19] using the NUS high-demagnification microprobe, enabling the production of high-resolution, high-contrast transmission channelling images.

* Corresponding author.
E-mail address: phymbhb@nus.edu.sg (M.B.H. Breese).

0168-583X/$ - see front matter © 2007 Elsevier B.V. All rights reserved.
doi:10.1016/j.nimb.2007.02.110

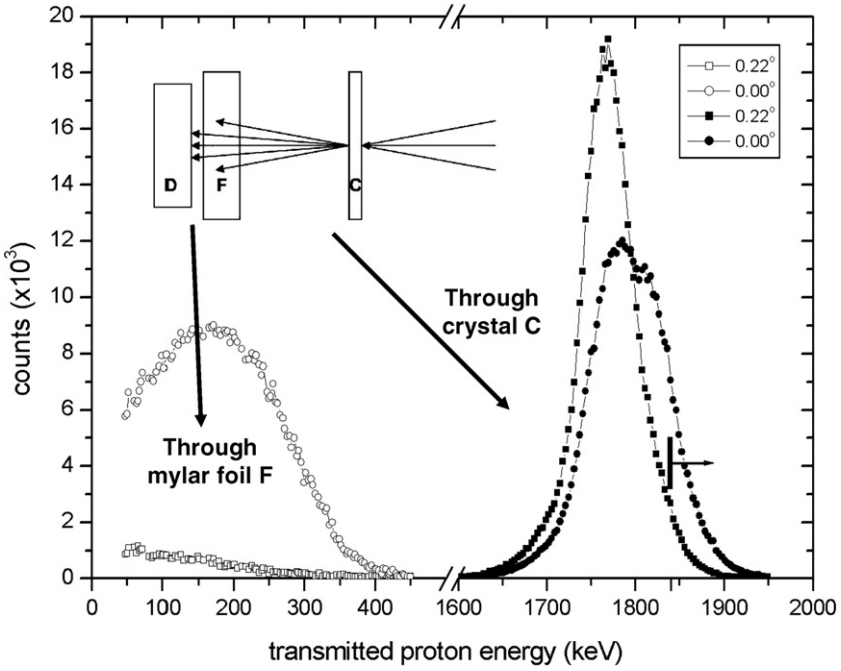

Fig. 1. Energy spectra of 2 MeV protons which are transmitted through a 10 μm thick [1 0 0] Si crystal (**C**) into a semiconductor detector (**D**) on the beam axis (solid symbols). Energy spectra are also shown after the beam passes through a 50 μm mylar foil (**F**) (open symbols). The lower energy threshold of ~1840 keV which this foil imposes on protons transmitted through it is shown by the arrow.

2. Improving the signal to noise level

The image contrast was greatly increased and the noise level reduced [19] by placing a foil in front of the semiconductor detector used to record the transmitted proton energies. Fig. 1 shows a (1 1 0) planar channelled and a random spectrum for 2 MeV protons transmitted through a 10 μm thick silicon wafer, without and with a mylar foil in front of the detector. Without the foil all protons are recorded in both random and channelled alignment, with a small increase in the energy observed for some protons in planar alignment owing to their lower rate of energy loss.

The foil thickness was chosen such that it stopped many lower-energy, dechannelled protons so with the foil in place only the longer range, high-energy planar channelled protons which remain channelled all the way through the sample are recorded. With the foil present, any defect-induced dechannelling causes significant contrast variations in the measured proton intensity, resulting in high-contrast, low-noise transmission channelling images. This measurement geometry also has the virtue of being compact and is simple to implement within the restricted geometry of a high-demagnification microprobe.

3. Altering the beam–crystal alignment

Planar alignment of the thin crystal is sufficient for most imaging requirements using transmission channelling since planar channelling is more sensitive to defect-induced dechannelling compared with axial alignment. The use of a microprobe provides several different alternatives to varying the beam–crystal alignment, other than use of a goniometer, for channelling analysis. Since there was little space in the chamber of the NUS high-demagnification microprobe to install a goniometer, other approaches to varying the beam–crystal alignment were explored. A beam-rocking system provides the ability to tilt a focused beam spot through angles of several degrees, with the beam remaining stable on the sample surface to within 2 μm [20]. Another solution is to shift the collimator slits of the microprobe away from the beam axis [21], resulting in the beam being tilted with respect to the crystal surface. A horizontal/vertical collimator displacement of 50 μm produced a change of 0.13°/0.04° respectively in the beam tilt with respect to the sample surface. With this procedure no loss of spatial resolution is observed in a beam spot size of 60 nm when the beam is tilted by up to 0.5°.

Care is needed however on high-demagnification systems because the beam angle significantly changes with scan position over the sample surface. This limits the maximum useable area over which an image can be recorded, and is much more extreme than on a low demagnification microprobe [22] (as demonstrated below in Fig. 5). This effect is shown in the transmission channelling image in Fig. 2, recorded from a 10 μm thick silicon crystal containing stacking faults. The bright band shows where the beam passed through planar channelling alignment, the dark regions on either side show where the beam is in a random alignment. To maintain the beam/crystal angular variation to a small fraction of the planar channelling critical angle means that the scan size in a transmission channelling image must be restricted to a few tens of microns. This

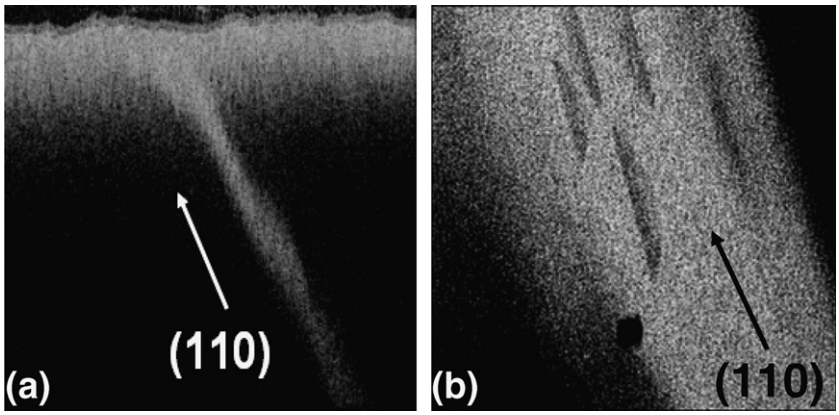

Fig. 2. Transmission channelling images recorded from the new high-demagnification microprobe over areas of (a) 1×1 mm^2 and (b) 50×50 μm^2. The bright diagonal band is due to the beam becoming aligned with the (1 1 0) planar channelling direction as the beam sweeps over the sample surface.

same process does however provide another means of visually locating the planar channelling location and another way of aligning the sample by introducing an offset in the beam scan position. This is similar to beam rocking though it does not require any additional scan coils.

4. Results

Fig. 3(a) shows a transmission channelling image of a stacking fault recorded with a low demagnification microprobe and a less efficient counting system in which all transmitted ions were measured, so the count rate is dominated by the nonchanneled protons which convey little useful information. Dark/bright regions represent regions of high/low energy loss respectively. Fig. 3(b) shows transmission channelling image of a single stacking fault in a [1 0 0] silicon wafer at a tilt of 0.10° to the vertically-running (0 1 1) planes, recorded on the new high-demagnification microprobe. Periodic intensity oscillations are observed as bright/dark bands and are fully discussed in [19], where the oscillation wavelength and the 'decoherence length' of the planar channelled protons are determined.

High-contrast transmission channelling images of isolated bunches and individual 60° misfit dislocations [23] in thick, partially-relaxed Si/$Si_{0.95}Ge_{0.05}$ layers were also recorded [24] and shown in Fig. 4. The optical DIC (differential interference contrast) image in Fig. 4(a) shows a cross-arm running along the (1 1 0) and (1 $\bar{1}$ 0) planes, and the transmission channelling images in Fig. 4(b)–(d) were recorded from within the boxed area. The wide, horizontally-running band produced by the bunch of five dislocations lies along the (1 1 0) planes, with two etch pits visible. A change in contrast is observed at the bunch of five dislocations, from dark in Fig. 4(b) to dark/bright in Fig. 4(d). All components of the Burgers vector of 60° dislocations were considered in [25] to interpret the above results.

5. Real-time imaging of lattice defects

The transmission channelling image shown in Fig. 3(b) took 45 min to collect with sufficient statistics, which was largely limited by the data acquisition counting rate of several kHz. In order to speed up data acquisition a new

Fig. 3. Transmission channelling images of stacking faults (a) was recorded with a low demagnification microprobe over a 40×40 μm^2 area with the old data collection geometry. The image in (b) was recorded using the high-demagnification microprobe with the new data collection geometry from a 3.3×3.3 μm^2 area close to the central fault portion of a stacking fault, indicated by the box in (a).

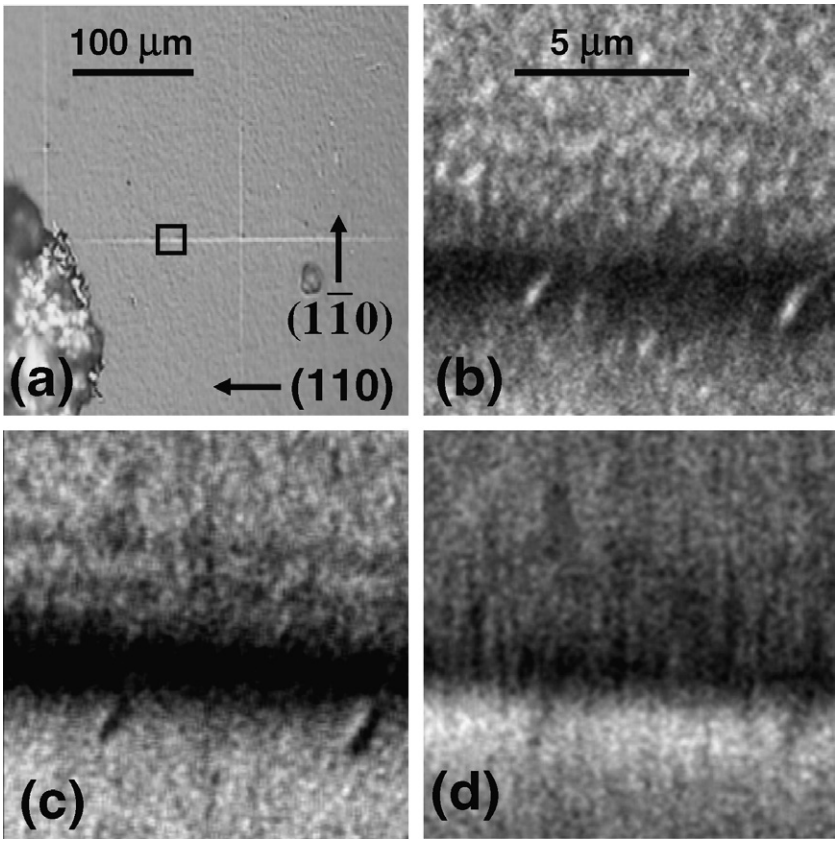

Fig. 4. (a) Low magnification optical DIC image. A marker of silver paint was placed at the left edge for subsequent location of this cross. (b)–(d) Transmission channelling images of the 11×11 μm^2 boxed area shown in (a). The two oval features are etch pits. Beam tilt angle to the (1 1 0) planes is (b) +0.16°, (c) 0.00°, (d) −0.16°.

measurement system was built which was capable of recording transmission channelling images in real-time and also providing a quick way to rapidly position regions of interest of the samples.

This was done by turning the low flux of high-energy planar channelled protons which pass through the mylar foil behind the sample into a continuous current of ion induced secondary electrons. The transmitted protons passed through a small aperture and then passed a stack of very thin carbon foils spaced 1 mm apart. This resulted in large numbers of secondary electrons produced from each carbon foil surface. The beam was stopped on a thick copper block which also generated further secondary electrons. This large secondary electron flux was extracted by applying an electric field transverse to the grids and accelerated onto a P47 plastic scintillator. The resultant light

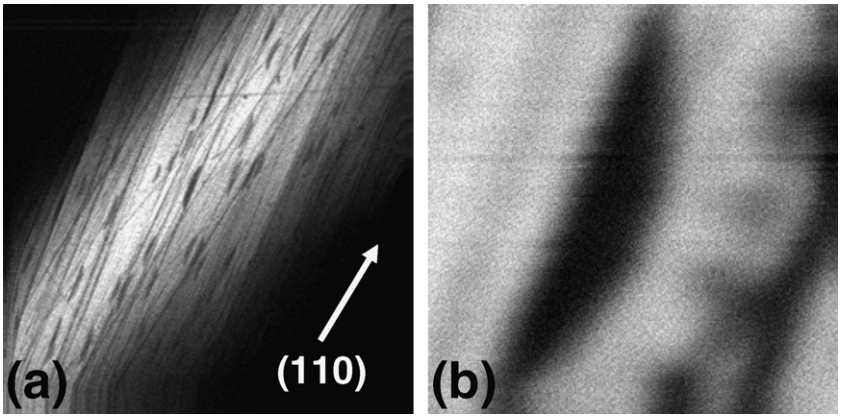

Fig. 5. Transmission channelling images of stacking faults recorded by displaying the variation in a continuous secondary electron flux produced by protons transmitted through the thin crystals. (a) 200×200 μm^2 area. (b) 40×40 μm^2 area. Dark represents regions of low measured secondary electron flux.

emission was recorded by a photomultiplier and turned into a continuous d.c. voltage as described in [25]. This measurement system relies on a stable proton beam current incident on the sample surface, which is provided by the NUS Singletron accelerator [26,27]. This can produce a beam on the sample surface which fluctuates by as little as 2% [28].

A higher proton beam current is required to produce transmission channelling images in this mode, typically a few pA, in order to generate a sufficiently large secondary electron flux. This measurement system was implemented on a low demagnification microprobe since there is no space in the sample chamber of the high-demagnification system. The spatial resolution of about 1 μm in the images is consequently low because of these two factors. Images were displayed by modulating a display screen with a brightness proportional to the recorded secondary electron intensity at each pixel, as shown in Fig. 5. Note the significant scan-induced dechannelling in Fig. 5(a) as the beam sweeps through (1 1 0) planar alignment. These images only required a few seconds to be generated and recorded and demonstrate the ability to produce real-time transmission channelling imaging of lattice defects.

6. Conclusions

A transmission channelling facility has been implemented on a high-demagnification microprobe. This requires special consideration of the way in which the beam–crystal alignment is varied, with several possible alternatives to the use of a goniometer. The measurement sensitivity has been greatly improved by only recording the high-energy channelled protons, resulting in transmission channelling images with lower statistical noise. This system has provided high-resolution, low-noise images of stacking faults and misfit dislocations in silicon wafers. A measurement system capable of providing transmission channelling imaging in real-time is described.

References

[1] M. Cholewa, G. Bench, G.J.F. Legge, A. Saint, Appl. Phys. Lett. 56 (1990) 1236.
[2] M. Cholewa, G. Bench, A. Saint, G.J.F. Legge, Nucl. Instr. and Meth. B 54 (1991) 397.
[3] P.J.C. King, M.B.H. Breese, G.R. Booker, P.R. Wilshaw, J. Whitehurst, G.W. Grime, F. Watt, M.J. Goringe, Nucl. Instr. and Meth. B 77 (1993) 320.
[4] M.B.H. Breese, P.J.C. King, J. Whitehurst, G.R. Booker, G.W. Grime, F. Watt, L.T. Romano, E.H.C. Parker, J. Appl. Phys. 73 (1993) 2640.
[5] J.C. Overley, R.C. Connolly, G.E. Seiger, H.W. Lefevre, Nucl. Instr. and Meth. 218 (1993) 43.
[6] M.B.H. Breese, J.P. Landsberg, P.J.C. King, G.W. Grime, F. Watt, Nucl. Instr. and Meth. B 64 (1992) 505.
[7] L.C. Feldman, B.R. Appleton, Phys. Rev. B 8 (1973) 935.
[8] D. Gemmell, Rev. Mod. Phys. 46 (1974) 129.
[9] D.V. Morgan (Ed.), Channeling: Theory, Observation and Applications, Wiley, 1973.
[10] L.C. Feldman, J.W. Mayer, S.T. Picraux, Materials Analysis by Ion Channeling, Academic Press, New York, 1982.
[11] M.B.H. Breese, P.J.C. King, P.J.M. Smulders, G.W. Grime, Phys. Rev. B 51 (1995) 2742.
[12] P.J.C. King, M.B.H. Breese, P.R. Wilshaw, G.W. Grime, Phys. Rev. B 51 (1995) 2732.
[13] P.J.C. King, M.B.H. Breese, P.J.M. Smulders, P.R. Wilshaw, G.W. Grime, Phys. Rev. Lett. 74 (1995) 411.
[14] M.B.H. Breese, D.N. Jamieson, P.J.C. King, Materials Analysis using a Nuclear Microprobe, Wiley, New York, 1996.
[15] M.B.H. Breese, D.N. Jamieson, J.A. Cookson, Nucl. Instr. and Meth. B 47 (1990) 443.
[16] G.W. Grime, F. Watt, Beam Optics of Quadrupole Probe Forming Systems, Adam Hilger, Bristol, 1984.
[17] F. Watt, J.A. van Kan, I. Rajta, A.A. Bettiol, T.F. Choo, M.B.H. Breese, T. Osipowicz, Nucl. Instr. and Meth. B 210 (2003) 14.
[18] J.A. van Kan, A.A. Bettiol, F. Watt, Nano Lett. 6 (2006) 579.
[19] M.B.H. Breese, E.J. Teo, M.A. Rana, L. Huang, J.A. van Kan, F. Watt, P.J.C. King, Phys. Rev. Lett. 92 (2004) 045503.
[20] D.G. de Kerckhove, M.B.H. Breese, G.W. Grime, Nucl. Instr. and Meth. B 129 (1997) 534.
[21] M.B.H. Breese, P.J.C. King, G.W. Grime, P.J.M. Smulders, L.E. Seiberling, M.A. Boshart, Phys. Rev. B 53 (1996) 8267.
[22] L.T. Romano, M.B.H. Breese, D.N. Jamieson, C. Chen, G.W. Grime, F . Watt, Phys. Rev. B 44 (1991) 6927.
[23] C.J. Gibbings, C.G. Tuppen, M. Hockly, Appl. Phys. Lett. 54 (1989) 148.
[24] M.B.H. Breese, L. Huang, E.J. Teo, P.J.C. King, P.R. Wilshaw, Appl. Phys. Lett. 87 (2005) 211907.
[25] M. Mazzer, A.V. Drigo, F. Romanto, G. Salviati, L. Lazzarini, Phys. Rev. B 56 (1997) 6895.
[26] E.J. Teo, M.B.H. Breese, A.A. Bettiol, F. Watt, L.C. Alves, J. Vac. Sci. Technol. B 22 (2004) 560.
[27] D.J.W. Mous, R.G. Haitsma, T. Butz, R.-H. Flagmeyer, D. Lehmann, J. Vogt, Nucl. Instr. and Meth. B 130 (1997) 31.
[28] J. Visser, D.J.W. Mous, A. Gottdang, R.G. Haitsma, Nucl. Instr. and Meth. B 231 (2005) 32.